

Quantum mechanical–rapid prototyping applied to methane activation

Richard P. Muller, Dean M. Philipp, and William A. Goddard III*

Materials and Process Simulation Center (139-74), California Institute of Technology, Pasadena, California, USA 91125

The accuracy of quantum mechanics (QM) calculations have improved to the point at which they are now useful in elucidating the detailed mechanisms of industrially important catalytic processes. This, combined with the continued dramatic decreases in the costs of computing (and the concomitant increases in the costs of experiments), makes it feasible to consider the use of QM in discovering new catalysts. We illustrate how to apply quantum mechanics to rapidly prototype potential catalysts, by considering improvements in the Catalytica Pt catalyst for activating methane to form methanol. The strategy is to first determine the detailed chemical steps of a prototype reaction (in this case, (bispypyrimidine)PtCl₂). Then, we identify critical conditions that must be satisfied for a candidate catalyst to be worth considering further. This allows the vast majority of the candidates to be rapidly eliminated, permitting a systematic coverage of large numbers of ligands, metals, and solvents to be covered rapidly, enabling the discovery of new leads. This Quantum Mechanics-Based Rapid Prototyping (QM-RP) approach is the computational-chemistry analogy of combinatorial chemistry and combinatorial materials science.

KEY WORDS: density functional theory; quantum chemistry; homogeneous catalysis; methane activation.

1. Introduction

There has been a revolution in Big Pharma, where experimental combinatorial syntheses are now used to develop rich libraries of compounds that can be rapidly sampled to discover new leads for drug development. Indeed, as discussed in Henry Weinberg's talk at the Grasselli Isee Conference, a similar experimental strategy has been developed by Symyx for rapidly prototyping new catalysts. We propose here a computational alternative for rapid prototyping and lead discovery of catalysts, which we refer to as *Quantum Mechanics-Based Rapid Prototyping* (QM-RP). This method is useful in suggesting novel catalysts with increased activity and selectivity. Combined with experimental verification, QM-RP should shorten the design cycle for developing industrially useful catalysts. We will outline the general strategy for QM-RP using low-temperature activation of CH₄ to form CH₃OH as an illustrative example.

The conversion of natural gas to liquid products such as alcohols is of great economic importance. The technologies currently practised in industry first involve conversion of CH₄ to syngas (carbon monoxide plus hydrogen), an energy-intensive, very high temperature (~850 °C) process. Fischer–Tropsch chemistry [1] is then used to produce the oxidized liquid products, which may be preceded by water-gas shift to obtain the best ratio of CO to H₂. Direct conversion through low-temperature catalysis would have many advantages; however, most current processes are plagued by low

yields and/or high catalyst costs [2–12]. The major challenge in developing such direct methods is that the C–H bond in the alkane substrate (e.g., methane) is very unreactive, whereas the desired partially oxidized products (e.g., alcohols) generated by direct catalytic pathways are usually more reactive than the starting alkanes. Thus, it is too easy to form products that are fully oxidized and commercially unimportant.

In 1993, Periana *et al.*, [13] then at Catalytica Corporation, reported an Hg system that selectively oxidized methane to methanol with a 43% one-pass yield. An even more effective Pt catalyst was reported in 1998 by Periana *et al.* [14] to convert methane to methanol with a 72% one-pass yield and 81% selectivity. This Pt catalyst consists of dichloro(η -2-{2,2'-bipyrimidyl})platinum(II) (hereafter referred to as bpym(Pt)Cl₂), shown in figures 1 and 2. It operates in concentrated super-dry (water-free) sulfuric acid (102%) at 220 °C. In sulfuric acid solvent, the product is the methyl bisulfate ester of methanol, requiring addition of water to form the product methanol. However, water (which is generated during the conversion process) inhibits the catalyst. This requires an expensive separation process that makes the overall economics unfavorable. Despite the practical problems, this system is very effective and selective for conversion of methane to methanol. Hence, we will use this system to illustrate the QM-RP approach.

Herein, we will focus on understanding the essential steps of the Catalytica Pt catalyst, where the most serious difficulties lie in generating a more active catalyst compatible with water. Our calculations have established that the mechanism of the Catalytica Pt catalyst involves C–H activation step, oxidation, and then functionaliza-

* To whom correspondence should be addressed.
E-mail: wag@wag.caltech.edu

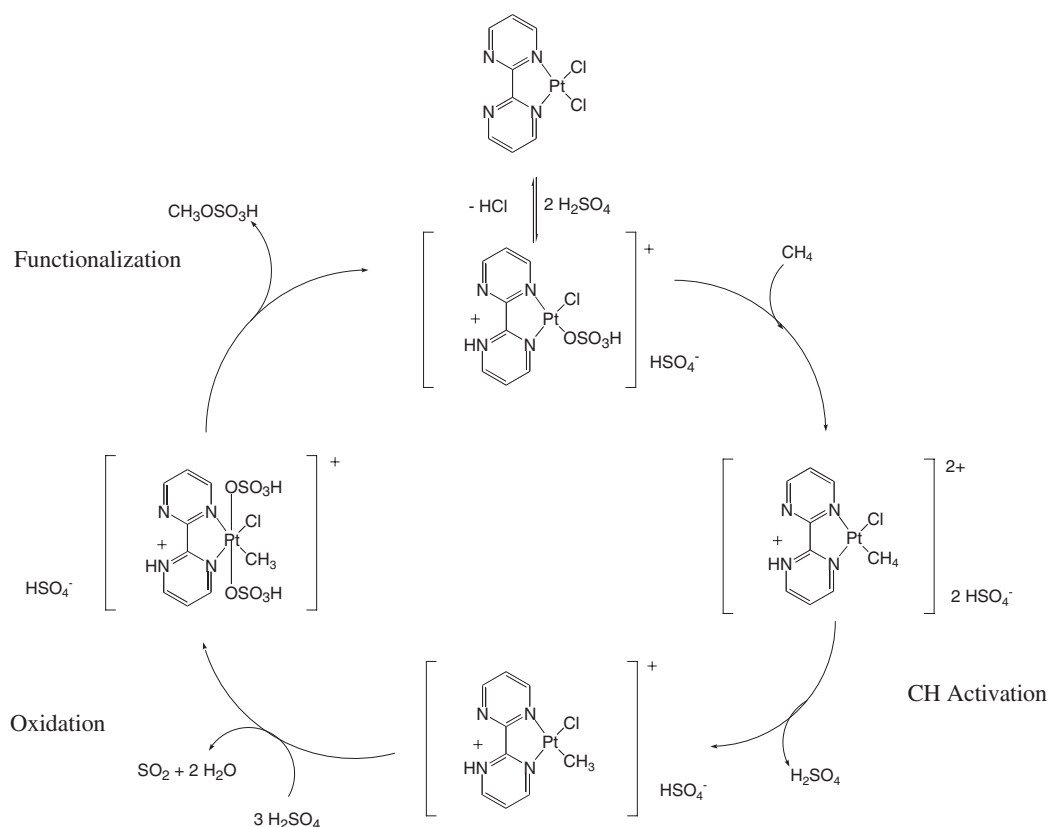


Figure 1. Mechanism of the catalytic cycle for the Catalytica Pt catalyst.

tion, as indicated in figure 1. Thus, we will consider complexes in which the Catalytica Pt catalyst has one chloride and one bisulfate ligand in addition to the bispyrimidine ligand. Previous studies indicate this to be the active form in the concentrated sulfuric acid solvent (after the first turnover, in which the second Cl ligand is “washed out” as HCl). We will concentrate here on the C–H activation step, since it is likely to become rate determining for less acidic solvents such as water (oxidation is observed to be rate determining for the Catalytica system in concentrated sulfuric acid [14]).

2. General strategy of QM-RP

The QM-RP strategy involves the following steps:

(1) Determine the most important reaction pathways (Mechanism) leading to the desired products and any other accessible side products:

- (a) First, we use *ab initio* quantum chemistry methods such as density functional theory (DFT) to optimize the various structures that might be relevant. These calculations include solvation effects on structure and energy. For complex ligands, the QM can be extended to include a force-field description of the parts of the system, remote from the catalytic center. This may involve mixed quantum mechanics/molecular mechanics (QM/MM) methodology.
- (b) Next, we determine the key intermediates and transition-state (TS) structures. Here, it is essential to ensure that the TS is a true saddle point (one negative curvature) and that the

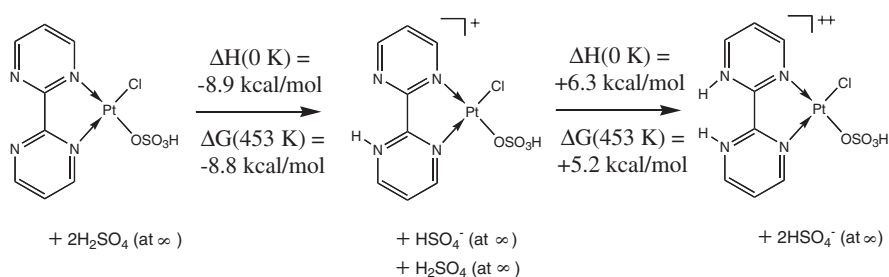


Figure 2. Comparison of the various levels of protonation (zero, one, and two protons) for the Catalytica Pt catalyst.

pathway is determined from each initial species to each product.

- (c) Finally, on the basis of these structures and energies, we elicit the mechanism and energy surface for the catalytic cycle.
- (2) Find catalytic bottlenecks
 - (a) Step 1 is applied first to any system for which there are already experimental results to determine the mechanism and energy surface.
 - (b) On the basis of the results of step 2(a), we identify the difficulties with the current catalysts and validate the theory by any available comparisons to experimental results. These difficulties include points where the catalyst is too slow or becomes poisoned (i.e., intermediates that are overly stable and/or transition-state structures that are too high in energy).
 - (3) Screening and lead discovery for new catalysts
 - (a) Starting with the knowledge of the bottlenecks in the current catalysts, we consider a variety of changes (of metal, ligand, co-catalysts, solvent, etc.) and examine how these changes affect the critical bottleneck. In this screening process, we do NOT redo the whole mechanism and energy surface. Rather, we narrow the field of good candidates by eliminating systems that fail a simple screening test. Such screening tests involve the calculation of only a small subset of the key intermediates and/or transitions and making simple comparisons of their relative energies to see if they fulfill some predetermined requirement. For example, if it is necessary for one intermediate to be lower in energy than another intermediate in order for a catalyst to be viable, then these two structures are calculated for each potential system. Cases with favorable comparisons move on to the more stringent tests in step 3(b). This process may take only a few percent of the effort to investigate the entire mechanism.
 - (b) For the few cases that satisfy the crucial bottleneck (reducing the activation barrier to a tolerable amount), we examine other potential problems such as poisoning, decomposition of an active state, or side reactions. The goal is to sift quickly through a large number of plausible candidates to eliminate with the least possible effort all systems with fundamental problems.
 - (c) Systems that pass through the filters in steps 3(a) and 3(b) will suggest possible leads worthy of a more systematic study. For these cases, we examine more carefully the various steps to obtain accurate barriers for side reactions or decomposition, etc.
 - (d) Steps 3(a) through 3(c) are repeated until promising catalysts are formulated. Variations include changing the metal, changing the ligand, changing the solvent, and stabilizing additives.
- (4) Refine catalysts
 - (a) As leads are developed for promising catalyst systems, we consider various refinements. These refinements might include adding sterically bulky groups and other minor variations to make the catalysts more stable or less sensitive to the environment.
 - (b) Fine-tuning can also be done to control the structure of the catalytic products (e.g., for polymerization of polar monomers, fine-tuning might optimize the production of highly isotactic or highly syndiotactic polymers and/or control how monomers are incorporated into copolymers).
 - (5) Experimental tests

As progress is made in developing new leads, experimental validation is important at various steps to ensure that unexpected but important steps have not been missed in the theory. In addition, as the refinements are made, it is important to emphasize systems that simplify the ultimate synthesis. However, RP-QM be carried out on 100 times more systems than the experimental.

3. Computational methods

All quantum-chemical calculations were carried out using the hybrid B3LYP flavor of DFT using the Jaguar (v4.0) program [15]. B3LYP includes non-local gradient corrections to the Slater local exchange functional [16] and some exact Hartree–Fock exchange. We use parameters [17] referred to as Becke 3 along with the Becke non-local gradient correction [18], the Vosko–Wilk–Nusair exchange functional [19], and the Lee–Yang–Parr local and non-local correlation functional [20]. We solve for the spin-restricted singlet states *without* spatial symmetry constraints.

The basis set used for Pt is the Hay and Wadt 18-electron relativistic effective-core potential [21]. For all other atoms, the 6-31G* basis set is employed, except for carbon atoms of the bipyrimidine ligand, for which the 6-31G basis set was used. Diffuse functions (6-31G* + basis set) are added to non-hydrogen atoms when modeling an anion separated at infinity, as well as the respective atoms in their conjugate acid.

All structures are geometry-optimized in solution, corresponding either to minima (zero negative eigenvalues for the Hessian) or to TS structures (one negative Hessian eigenvalue). Transition-structure searches are guided by a quadratic synchronous transit method,

employing both reactant and product geometry to aid in the search along a reaction coordinate. The zero-point energy corrections are computed from vibrational frequencies determined for analytical vacuum Hessians at the solution-phase optimized geometries. These same vibrational frequencies are used for the finite-temperature enthalpy and entropy corrections included in free-energy values.

As all of these calculations include solvation effects, we use the Poisson–Boltzmann continuum model (PBF) [22–24] available within the Jaguar (v4.0) program. The implementation of this method is the same as that used by Philipp *et al.* [25]. As was the case in that reference, no explicit solvent molecules or counterions are used in this study, with the same rationalizations being relevant here. Concentrated sulfuric acid (102%) is the solvent used with the Catalytica Pt catalyst for methane activation [14]. Consequently, our calculations incorporating solvent effects assume parameters appropriate for such a solvent (dielectric constant of $\epsilon = 98$ for 99% sulfuric acid [26] and a probe radius of 2.205 \AA).¹

All energies are reported as enthalpies at 0 K [ΔH (0 K)] with zero-point energy but without finite-temperature enthalpy or entropy corrections. Additionally, free energies [ΔG (453 K)] are reported that include finite-temperature enthalpy and entropy corrections to 453 K for the thermodynamic results comparing the various levels of protonation for the active Catalytica Pt catalysts.

4. Mechanism of methane activation by the Catalytica Pt–bpym catalyst

4.1. C–H activation

Before modeling C–H activation, it is essential to establish the degree of protonation of the bipyrimidine ligand complexed to Pt in sulfuric acid. The results (figure 2) show that transfer of a proton from a solvated sulfuric acid to the unprotonated Pt catalyst is enthalpically exothermic by $8.9 \text{ kcal mol}^{-1}$ at 0 K. Transfer of another proton from a sulfuric acid is endothermic by $6.3 \text{ kcal mol}^{-1}$ of enthalpy. These proton transfers respectively release $8.8 \text{ kcal mol}^{-1}$ and require $5.2 \text{ kcal mol}^{-1}$ of free energy at 453 K. Thus, the one-proton case is the important species under reaction conditions. However, all three levels of protonation must be considered in modeling C–H activation, since they may play a role in various intermediates or in modified solvents.

The results for the C–H activation step calculations with the zero-proton case are shown in figure 3. The barrier from structure **A** to structure **B** has an activation barrier of $30.2 \text{ kcal mol}^{-1}$ (transition-state structure **T1**), with a reaction enthalpy of $28.7 \text{ kcal mol}^{-1}$ of energy. The geometry of **T1** reveals that this mechanistic step is associative, with a bisulfate ligand leaving as the methane comes in to form an agostic hydrogen interaction at the coordination site being vacated by the bisulfate. Structure **B** is a methane-complex intermediate with the dissociated bisulfate solvated in the proximity.

From intermediate **B**, two reasonable pathways can lead to H abstraction to form the methyl complex.

The oxidative-addition pathway (which has been established to be important in the Shilov reaction) involves the formation of a Pt–H bond simultaneous with the forming of a Pt–methyl complex. This transition-state structure **T2b** shows a clear Pt–H bond with Pt–H distance of 1.6 \AA (see figure 5 for the analogous one-proton case structure). The solvated bisulfate aids in this step. Another bisulfate from solution could coordinate in the axial position opposite the axial position to which the hydrogen is migrating; however, this makes little energetic difference for the transition barrier of $36.6 \text{ kcal mol}^{-1}$.

We find that electrophilic substitution leads to a much lower barrier. In this mechanism, a bisulfate plucks off the methane hydrogen involved in the agostic interaction with the Pt to form sulfuric acid and structure **C**, which is $17.2 \text{ kcal mol}^{-1}$ higher in energy than the initial structure **A**. The bisulfate used here is the one that dissociated from structure **A**, but any bisulfate from solution might also be involved. The transition barrier for electrophilic substitution is $34.2 \text{ kcal mol}^{-1}$, the relative energy of transition-state structure **T2**. The Pt–H distance in structure **T2** is 1.9 \AA , while the O–H distance is 1.4 \AA , indicating that a Pt–H bond is not being formed (see figure 5 for the structures obtained for the one-proton case; these are all very similar to the structures for the zero-proton and two-proton cases).

As the barrier for oxidative addition is calculated to be larger than that for electrophilic substitution, we conclude that the Catalytica Pt catalyst operates through electrophilic substitution.

Figure 4 displays the results of C–H activation modeling for the Catalytica Pt catalyst with one proton added to the bipyrimidine ligand, while figure 5 shows the actual solution-phase optimized structures obtained from the modeling. The proton is bonded to the backside nitrogen that is on the same side of the Pt as the bisulfate ligand, as this location leads to the lowest energy for structure **A** (see structure **A** in figure 5). We see that the methane-complex intermediate **B** is now $27.4 \text{ kcal mol}^{-1}$ higher in energy than the initial structure **A** and clearly has an agostic hydrogen interaction present, as evidenced by the 1.911 \AA Pt–H

¹Probe radius r_{solv} is calculated from $r^3 = 3m\Delta/4\pi\rho$ ($10^{24} \text{ \AA}^3 \text{ cm}^{-3}$), where m is the molecular mass obtained by dividing the molecular weight [28] in g mol^{-1} by Avogadro's number, Δ is the packing density (assumed to be 0.5 owing to lack of detailed knowledge of liquid structure), and ρ is the density in g cm^{-3} at 20°C [28].

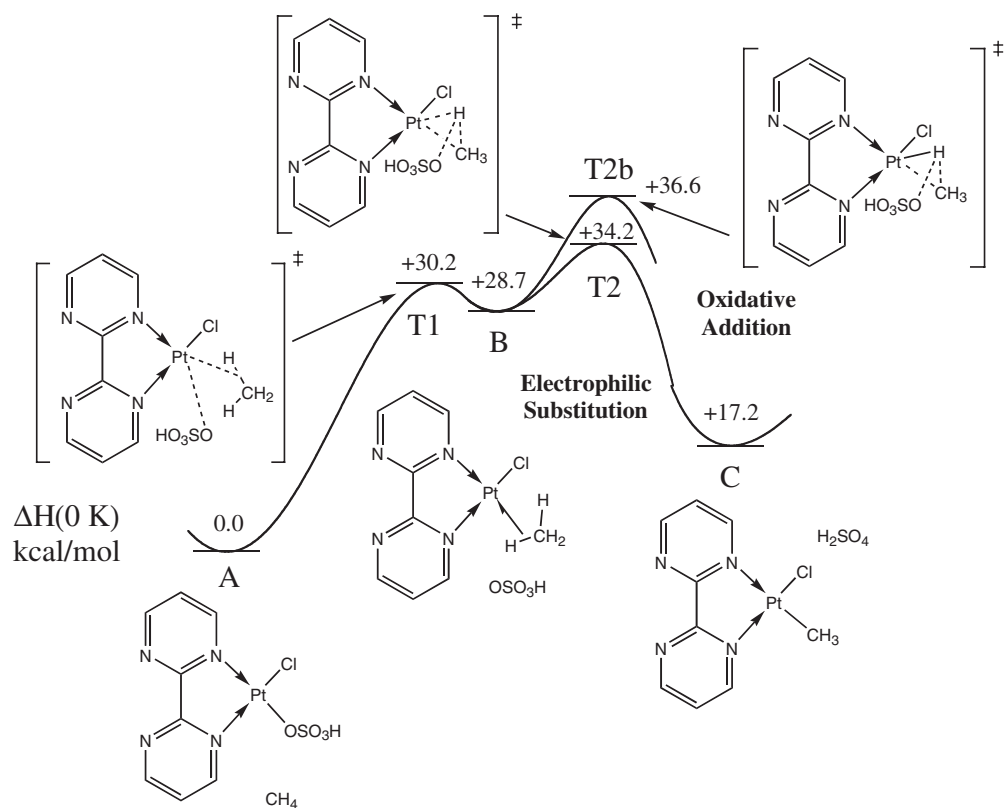


Figure 3. Solution-phase potential energy diagram for the C–H activation of the Catalytica Pt catalyst with *zero* added protons.

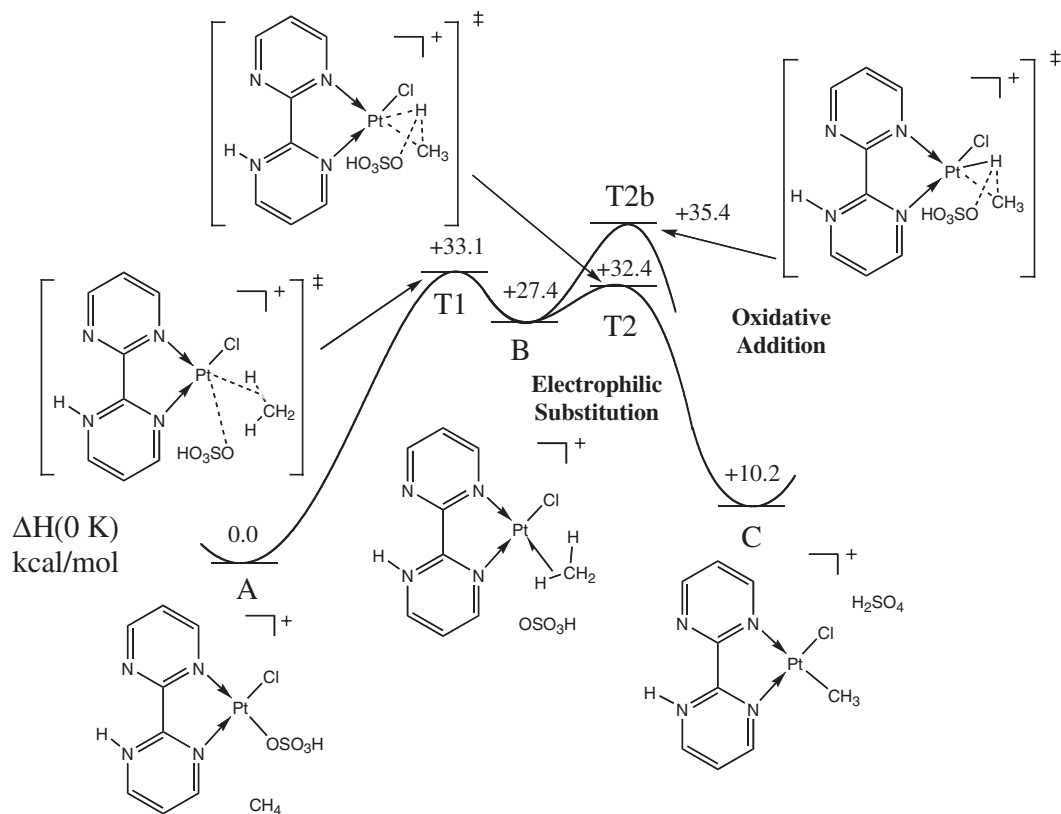


Figure 4. Solution-phase potential energy diagram for the C–H activation of the Catalytica Pt catalyst with *one* added proton.

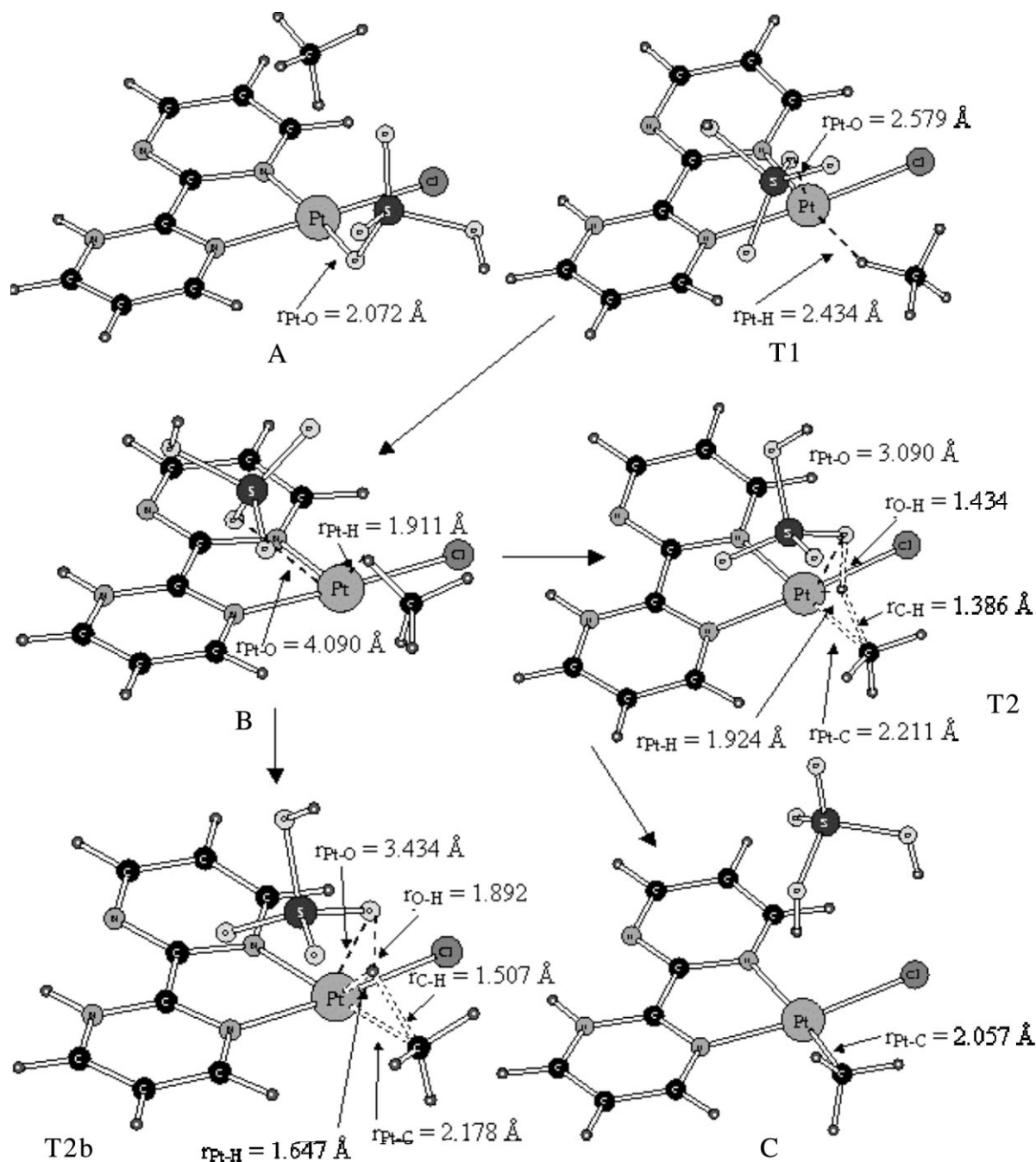


Figure 5. Solution-phase optimized structures involved in the C-H activation of the Catalytica Pt catalyst with *one* added proton.

distance for structure **B** in figure 5. The formation of the methane complex has an activation barrier of $33.1 \text{ kcal mol}^{-1}$ for **T1** and is associative, as seen by the transition-state structure **T1** in figure 5. From **B**, electrophilic substitution is again preferred, with the transition barrier for **T2** computed to be $32.4 \text{ kcal mol}^{-1}$, as compared to $35.4 \text{ kcal mol}^{-1}$ for the oxidative-addition transition-state structure **T2b**. In viewing the structures displayed in figure 5, it is clear that a Pt-H bond is being formed for structure **T2b**, as the Pt-H distance is 1.647 \AA . Such a bond is not formed in **T2**, where the Pt-H distance is 1.924 \AA , as the H is

bonding to one of the oxygen atoms of the bisulfate (the O-H distance for **T2** is 1.434 \AA).

Of special note here is that the barrier for methane complexation, **T1**, is slightly higher than the barrier to form the methyl complex through electrophilic substitution, **T2**. This result agrees with the experimental observations of Periana *et al.* [14] that at temperatures too low to form oxidized product, methane in deuterated sulfuric acid undergoes multiple-deuterium exchange. We interpret this as repeated transitions from **B** to **C** and back before dissociation of **B** to **A** occurs. This requires that **T1** > **T2**.

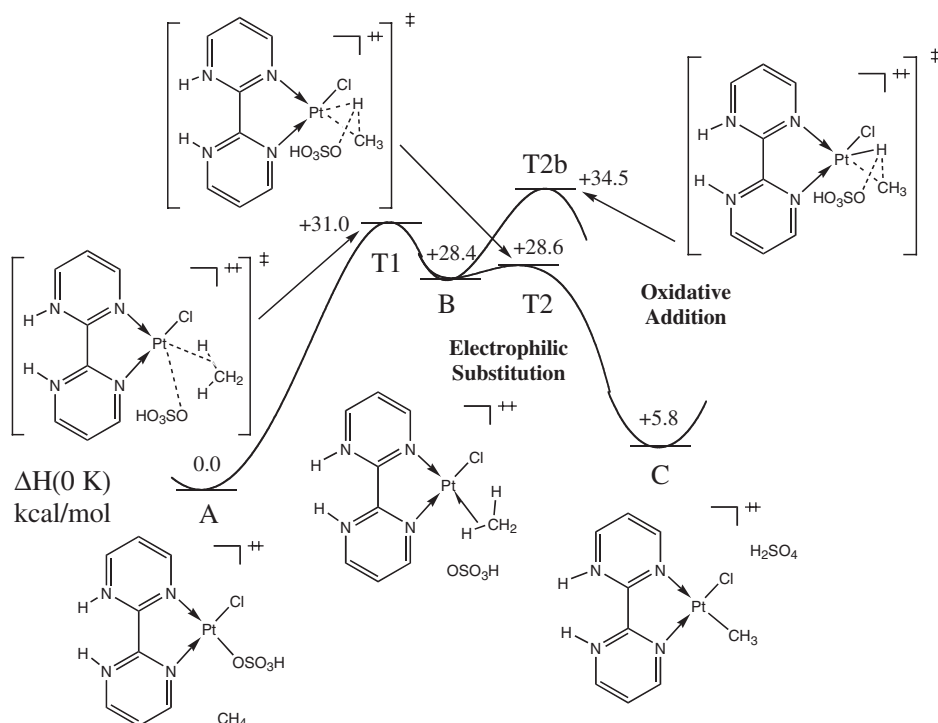


Figure 6. Solution-phase potential energy diagram for the C–H activation of the Catalytic Pt catalyst with *two* added protons.

C–H activation for the case with two protons added to the bipyrimidine ligand of the Pt catalyst is illustrated in figure 6. The methane complex of structure **B** is found to be $28.4 \text{ kcal mol}^{-1}$ less stable than the initial structure **A**, needing $31.0 \text{ kcal mol}^{-1}$ of energy to overcome the barrier **T1**. We again see that electrophilic substitution is the preferred pathway in forming the methyl complex of structure **C** from **B**. The transition barrier for **T2** is $28.6 \text{ kcal mol}^{-1}$, which is much lower than the oxidative-addition transition-state barrier of $34.5 \text{ kcal mol}^{-1}$ for **T2b**. It is also noted that **T1** is again greater than **T2** (31.0 vs. $28.6 \text{ kcal mol}^{-1}$).

Analyzing the above results indicates some salient trends for C–H activation.

- Increased protonation makes the metal more positive, making it more difficult to replace the bisulfate with an incoming methane (**T1** becomes larger).
- Increased charge on the metal environment favors oxidative addition and electrophilic substitution, i.e., **T2** and **T2b** become smaller. Likewise, the methyl-complex structure **C** becomes more stable relative to the initial structure **A**.
- As the degree of protonation is increased, **T1** becomes larger relative to **T2**, with the two most likely levels of protonation (one and two protons) having **T1** > **T2** (which is consistent with the experiment).

4.2. Functionalization

The potential energy diagram summarizing the mechanism for functionalization is shown in figure 7.

Here, we start with structure **M**, which is the likely complex after oxidation. Structure **M** has two bisulfate ligands in the axial coordination sites. We find that one of these must dissociate from the Pt to form a five-coordinate complex before the functionalization step can proceed. As this dissociation occurs, the methyl group (located in an equatorial site) simultaneously moves into the axial site vacated by the leaving bisulfate and the other axial bisulfate migrates into the equatorial site that had been occupied by the methyl group. The transition-state structure **T_{f1}** has a barrier of $26.4 \text{ kcal mol}^{-1}$ and is rate-determining for the functionalization step before yielding structure **N**, which is $0.2 \text{ kcal mol}^{-1}$ less stable than **M**.

Functionalization then proceeds by a bisulfate from solution (such as the just dissociated bisulfate, as is used here) reacting with the methyl group to form methyl bisulfate plus the product **O**. Structure **O** is $19.4 \text{ kcal mol}^{-1}$ downhill in energy from structure **M** and is just the regenerated initial complex **A** for the C–H activation step. This last step is analogous to an S_N2 reaction, where the Pt catalyst coordinated to the methyl group acts as a leaving group and is substituted by the bisulfate. This reaction has a barrier of $7.8 \text{ kcal mol}^{-1}$ for transition-state structure **T_{f2}**.

4.3. Water inhibition

We start with the Catalytic Pt catalyst in anhydrous sulfuric acid; however, water is produced as a by-product during the conversion of methane to methyl

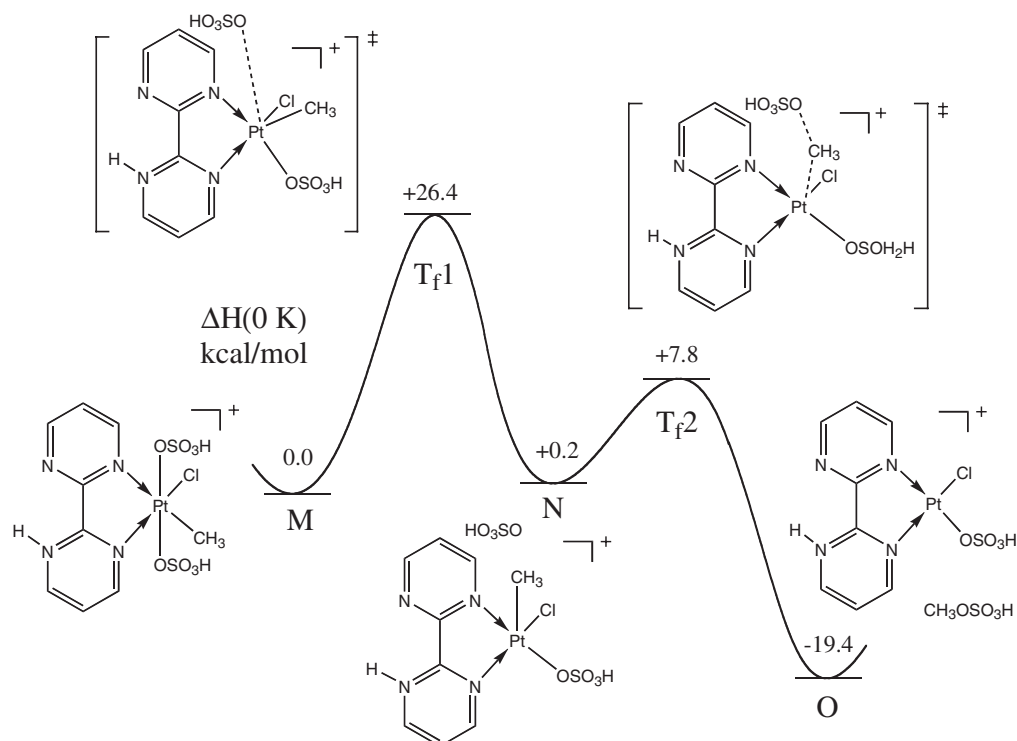


Figure 7. Solution-phase potential energy diagram for the functionalization of the Catalytica Pt catalyst. The case with one added proton is used.

bisulfate/methanol. This water is observed to further slow catalytic activity [14], ultimately poisoning the catalysts. Figure 8(a) shows the origin of this. Replacing the bisulfate ligand of the active complex on the left with

water lowers the enthalpy at 0 K by 6.8 kcal mol⁻¹. This means that water stabilizes the ground state catalyst species increasing the barrier for the C–H activation and subsequent steps.

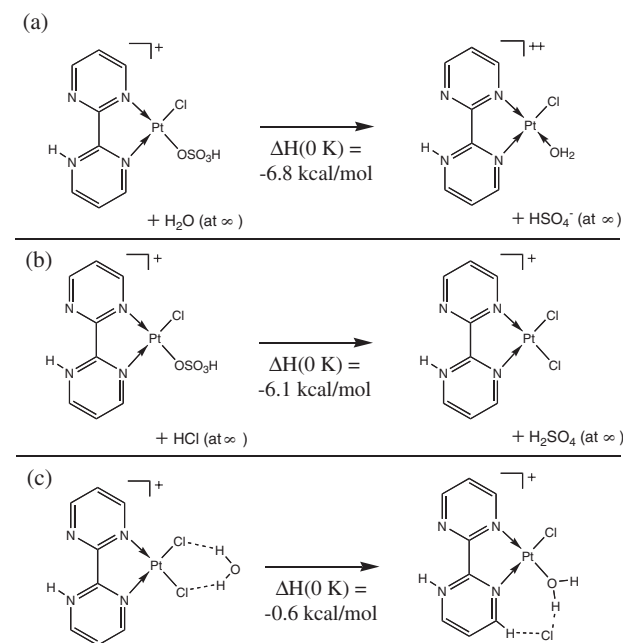


Figure 8. Thermodynamics of water inhibition for the Catalytica Pt catalyst. Ligand exchange of a bisulfate (OSO₃H) for the H₂O is shown in (a). In (b), exchange of a bisulfate for Cl is revealed, while (c) demonstrates the exchange of a Cl for H₂O₂ where the uncomplexed H₂O/Cl is kept in the immediate proximity.

Further corroboration of a ground state effect for water inhibition is revealed in figure 8(b), where exchange of a bisulfate ligand with a chloride ligand is downhill by 6.1 kcal mol⁻¹. Calculations done by Kua *et al.* [28] describe modeling of the Catalytica Pt catalyst with two chloride ligands (instead of one chloride and one bisulfate). The results of these studies show that this two-chloride form has much higher barriers (about 44 kcal mol⁻¹ for the analogous T1 barrier) for the C–H activation, and thus such a complex would be far slower than the case with bisulfate replacing a chloride.

Indeed, figure 8(c) shows that it is even enthalpically downhill (by 0.6 kcal mol⁻¹) to replace a chloride ligand for the complex on the left with water. This makes water poisoning even more unfavorable than it was for the two-chloride Catalytica Pt catalyst.

4.4. Summary

We have modeled the C–H activation and functionalization steps for methane conversion to methyl bisulfate by the Catalytica Pt catalyst. We find that methane complexation occurs via an associative mechanism leading to a methane-complex intermediate, which involves an agostic hydrogen interaction to the Pt. We find that the methane adds through electrophilic

substitution (preferred over the oxidative-addition pathway). For the most important level of protonation for the bispyrimidine ligand (one proton), the methane complexation is slower than the methane addition to form the methyl complex (i.e., **T1** > **T2**). Trends were also identified as the level of protonation increased from zero to one and then to two protons:

- As the degree of protonation increases (and thus the metal environment becomes more positive), it generally becomes more difficult to replace the bisulfate ligand with methane (the barrier for **T1** becomes larger).
- As the metal environment become more positive, electrophilic substitution (as well as oxidative addition) becomes easier. That is, **T2** (and **T2b**) become smaller.
- The methyl complex (structure **C**) becomes more stable relative to the initial active catalyst species **A** as the degree of protonation increases.

For functionalization, we found that an axial bisulfate must first dissociate before the methyl group can be eliminated as methyl bisulfate. This production of methyl bisulfate, as well as the regeneration of the initial active catalyst species, occurs through a mechanism analogous to an S_N2 reaction.

We found that water inhibition arises from stabilization of the ground state energies. Finding a catalyst that is sufficiently active enough to overcome water inhibition and which can operate in less acidic media (and ideally that of water) is paramount to development of a commercially viable methane conversion catalyst.

5. QM-RP studies

The mechanistic understanding outlined in the previous section suggests a strategy for QM-RP studies:

- (1) Determine the energy difference between the catalyst resting state and the C–H activation product. This is the difference between structures **A** and **C** in figure 4. Our goal is to surpass the Catalytica catalyst, so that we seek a system that has an energy difference of less than 10 to 20 kcal mol⁻¹. We eliminate without further study systems that are much less favorable than the Catalytica system. The structures **A** and **B** are locally quite stable, making the QM calculations quite fast. Thus, we may rapidly consider a very large number of potential catalysts. To speed up this process, the optimization of structures is done in vacuum, with solvation being used only for the optimum structure. However, cases that satisfy our cutoff (10 to 20 kcal mol⁻¹) may be optimized in solvent.
- (2) For systems with a favorable step 1, we consider the possibility of water poisoning. An effective catalyst should be resistant to inhibition by the products

(water and methanol). Thus, we consider reaction (a) in figure 8 and seek systems for which this reaction is energetically uphill (> 0). This again is a relatively fast calculation so that many systems can be considered.

- (3) For systems that pass steps 1 and 2, we compute the barriers for C–H activation (structures **T1** and **T2** from figure 4). Since our goal is to surpass the Catalytica system, we seek structures with barriers of less than 33 kcal mol⁻¹.
- (4) For systems that pass steps 1–3, we then determine the energetics and barriers for the oxidation and functionalization steps (figure 1). We may also consider a variety of solvents.
- (5) Systems that pass steps 1–4 are considered realistic targets for experimental synthesis and characterization. Here, we may consider modifications of the ligands to optimize stability.

To illustrate this process, we report some results in which we considered the Brookhart tridentate ligand used successfully for catalytic polymerization of ethylene (figure 9(a)), but we will optimize it for CH₄ activation. Here, we examined replacing the N atoms (that in the Brookhart catalyst form donor–acceptor bonds to the metal atom) with C, O, P, S, and other atoms to vary the ligand environment experienced by the metal atom. We also examined variation of this system (figure 9(b)) in which the donor ligands form formal covalent bonds to the metal.

Figure 10 shows two candidate structures. Both contain 16 electron Pt(II) systems. Structure (a) uses N, C, N atoms to coordinate the metal, but the C–Pt bond is covalent rather than donor–acceptor. Structure (b) uses three N atoms to coordinate the metal, where one of the N–Pt bonds is a formal covalent bond (considered as resonating between the left and right nitrogens). However, both cases lead to a very unfavorable ΔE (A–C) (51.3 and 34.6 kcal mol⁻¹, respectively). Since neither structure passes test 1 of QM-RP, we rejected them without further ado.

Figure 11 shows the same ligand system but with an Ir (III) system. In figure 11(a), we see that the system passes QM-RP test 1 in that it has a favorable ΔE (A–

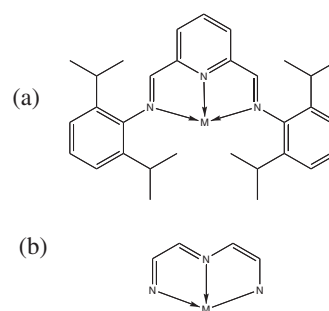


Figure 9. (a) Tridentate ligands used as templates for QM-RP variations. (b) A variation of this ligand that contains one covalent bond and two donor–acceptor bonds.

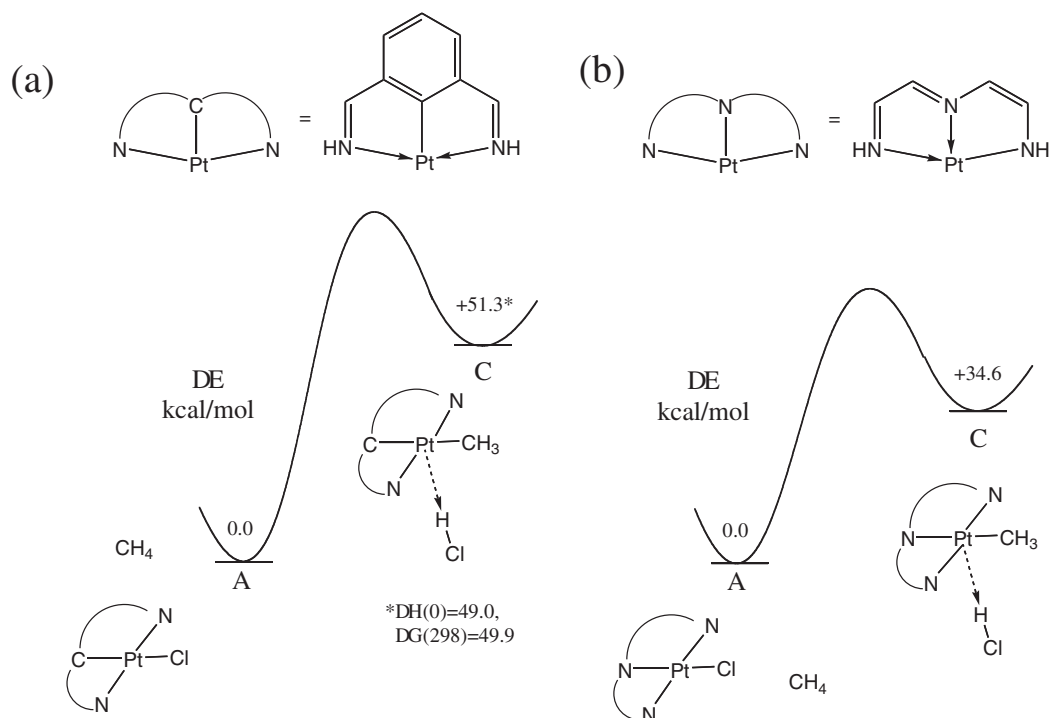


Figure 10. 16-electron ligand-system test cases for QM-RP of methane activation catalysts. Structure (a) uses N,C,N atoms to coordinate the metal and structure (b) uses N,N,N atoms to coordinate the metal. The metal in both cases is Pt(II). The reaction energetics for A to C are 51.3 and 34.6 kcal mol⁻¹, so that neither structure passes the first step of the QM-RP process.

C). Figure 11(b) shows that the overall energetics for this transformation are similarly favorable.

Figure 12 shows two additional candidates, again 16-electron Pt(II) systems, this time with NON (structure (a)) and OOO (structure (b)) coordinating atoms. Again, $\Delta E(A-C)$ is too high to pass QM-RP test 1 (22.5 and 18.0 kcal mol⁻¹ respectively). Thus, these structures were not considered further.

Figure 13 shows ligand systems with N,C,N coordinating atoms. Structure (a) uses an Os(II) metal atom, leading to a 14-electron complex. This leads to $\Delta E(A-C) = 32.7$ kcal mol⁻¹. Hence, it does not pass QM-RP test 1.

In contrast, structure (b) uses a Pt(II) atom, leading to an 18-electron system. Here, the $\Delta E(A-C) = 8$ kcal mol⁻¹, and thus it passes QM-RP test 1 and is a

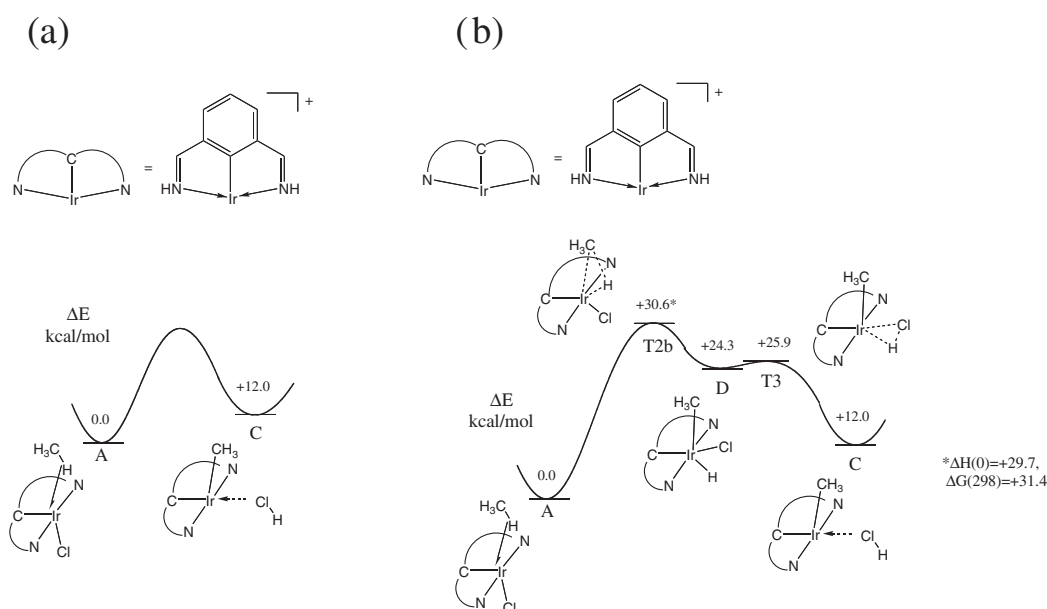


Figure 11. (a) Ir(III) system that passes QM-RP test 1; (b) the same ligand system showing a favorable activation barrier.

candidate for further study. Thus, we determined the transition state for the structure in figure 13(b), as shown in figure 14. The barrier to the C–H bond formation step is $48.9 \text{ kcal mol}^{-1}$, and thus, this candidate does not pass QM-RP test 3. (Note that the energy of structure **C** in figure 14 is $4.5 \text{ kcal mol}^{-1}$, whereas it was 8 kcal mol^{-1} in figure 13; this is the result of further optimization.)

Figure 15 shows a system similar to figure 14's system, but with a slightly different ligand at the center, having a Fischer carbene as the central carbon in the ligand system. This time, the barrier for the transformation from **A** to **C** is favorable ($32.5 \text{ kcal mol}^{-1}$). Unfortunately, the system is poisoned by water.

Figure 16 shows an Ir(III) structure that passes QM-RP tests 1 and 2. The $\Delta E(\text{A}-\text{C})$ is $15.6 \text{ kcal mol}^{-1}$, which is close enough to our target of $10.2 \text{ kcal mol}^{-1}$ to warrant further study. Moreover, the barrier is $33.7 \text{ kcal mol}^{-1}$, close enough to the target to make the system interesting. Unfortunately, the system reacts very exothermically with water (23 kcal mol^{-1}), and thus this system does not pass QM-RP test 3.

Figure 17 shows the same NCN ligand system with a Fischer carbene in the middle. Figure 17(a) shows Ir (I) (in contrast to Ir (III) in Figure 16), and Figure 17(b) shows Os (II) bound to the ligand. Neither system has favorable energetics for QM-RP test 1.

Figures 18–20 show resonating bidentate ligands, in which the ligand forms one covalent bond and one donor–acceptor bond to the metal. Figure 18 shows one such ligand bound to (a) Pt (II) and (b) Pt (IV). The Pt (II) compound does not have favorable energetics, whereas the Pt (IV) system does have favorable energetics, although it may ultimately be defeated as a methane-activation catalyst because it does not have another accessible oxidation state. Figure 19 shows the same ligand system with Ir (III), which does not have favorable energetics for QM-RP test 1. Figure 20 shows two different moieties for Au (III) that have surprisingly favorable energetics for QM-RP test 1.

Figures 21 and 22 show Ir systems of different oxidation states using classic Brookhart bidentate ligands. These systems are generally not resistant to water poisoning. Interestingly, though, figure 22 shows the formation of a methylene bond to the metal. Figures 23 and 24 show ligand systems with Ir (I) that are, in fact, resistant to water poisoning. As was the case in figure 22, figure 23 shows the formation of a methylene bond. Figure 24 is a slight variation on the ligand system in figure 23, and this time shows a more favorable bond to methyl than methylene.

Similar studies were carried out for over 100 cases. This led to several cases, which passed all three tests and which are being investigated experimentally.

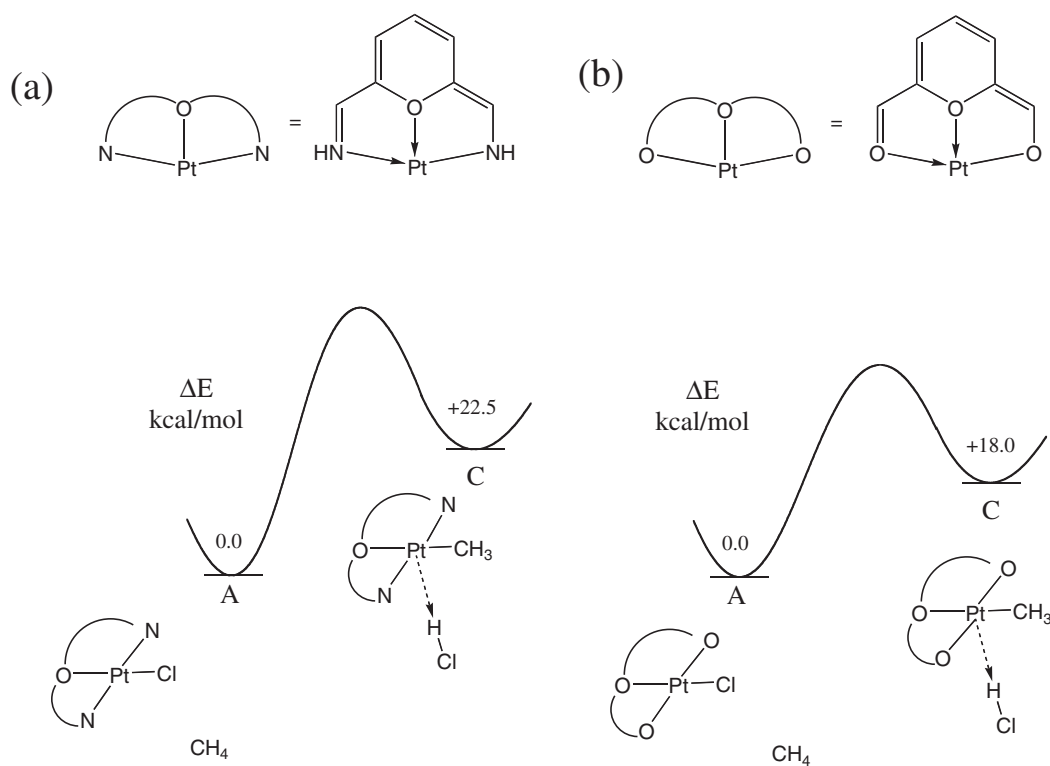


Figure 12. 16-electron Pt(II) complexes with N,O,N (a) and O,O,O (b) coordinating atoms. Again, as the $\Delta E(\text{A}-\text{C})$ energies are 22.5 and $18.0 \text{ kcal mol}^{-1}$ respectively, these systems do not pass QM-RP test 1 and are not pursued further.

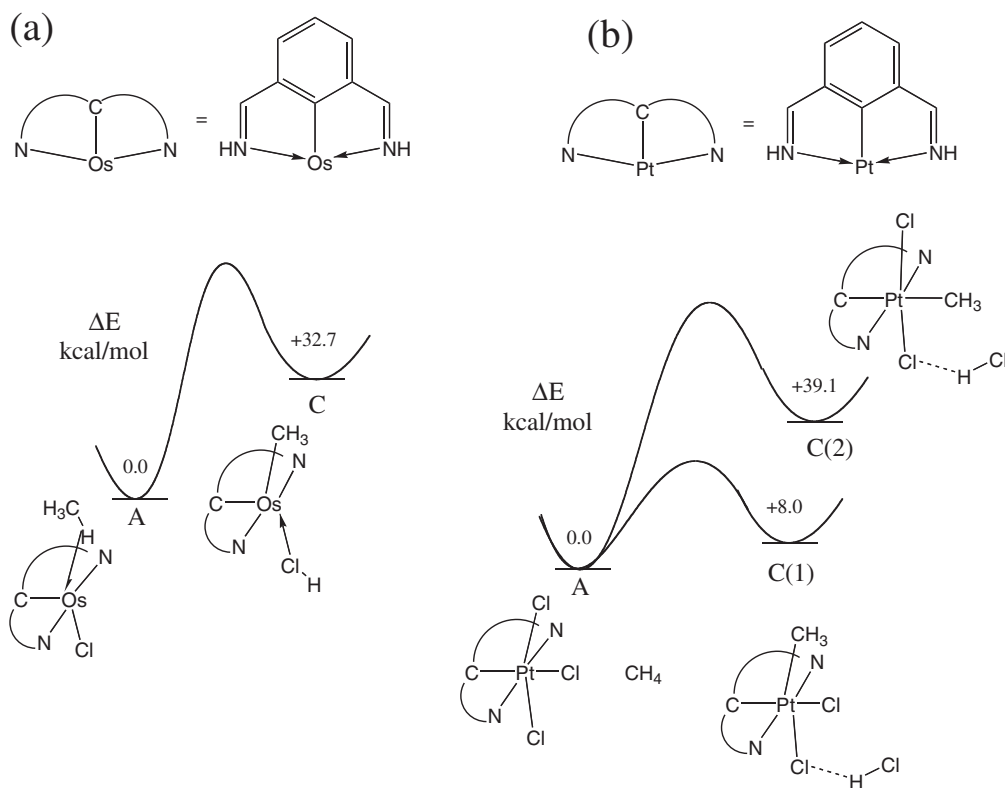


Figure 13. NCN structures with (a) Os(II) (14 electrons) and (b) Pt(II) (18 electrons). Structure (a) has a $\Delta E(A-C)$ of $32.7 \text{ kcal mol}^{-1}$, which does not pass QM-RP test 1, but structure (b) has $\Delta E(A-C)$, which does pass QM-RP test 1.

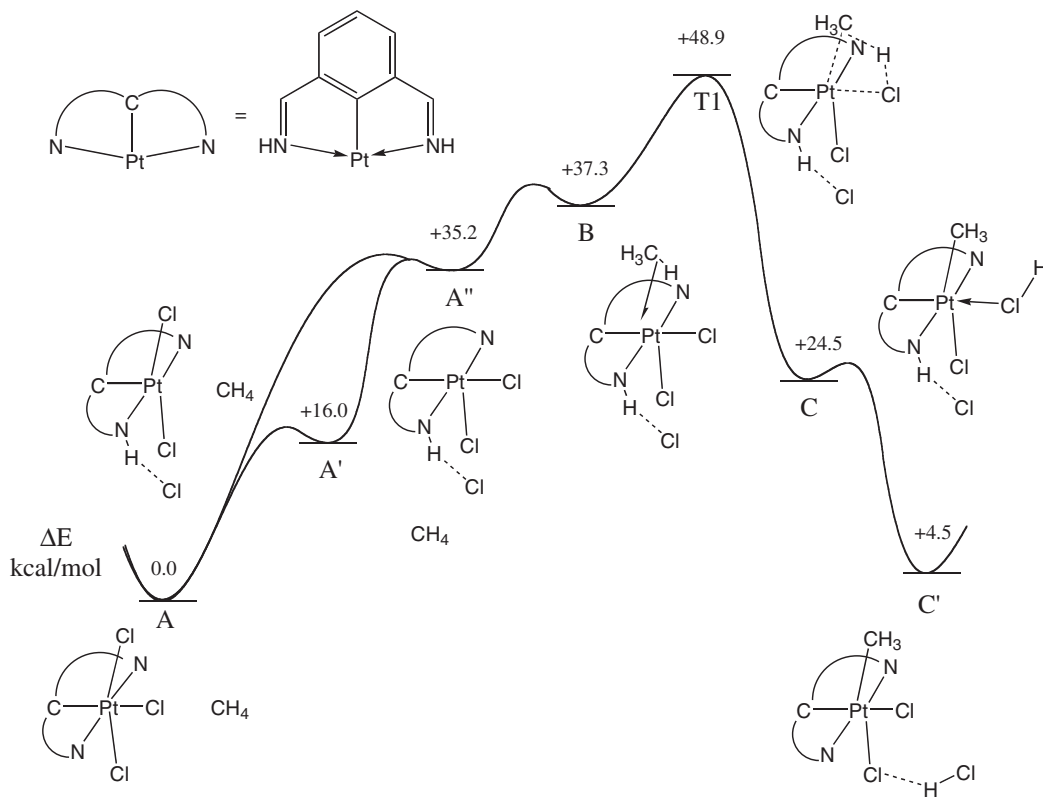


Figure 14. Transition state for C-H bond activation for the structure from figure 13(b). The barrier is $48.9 \text{ kcal mol}^{-1}$, and thus does not pass QM-RP test 2.

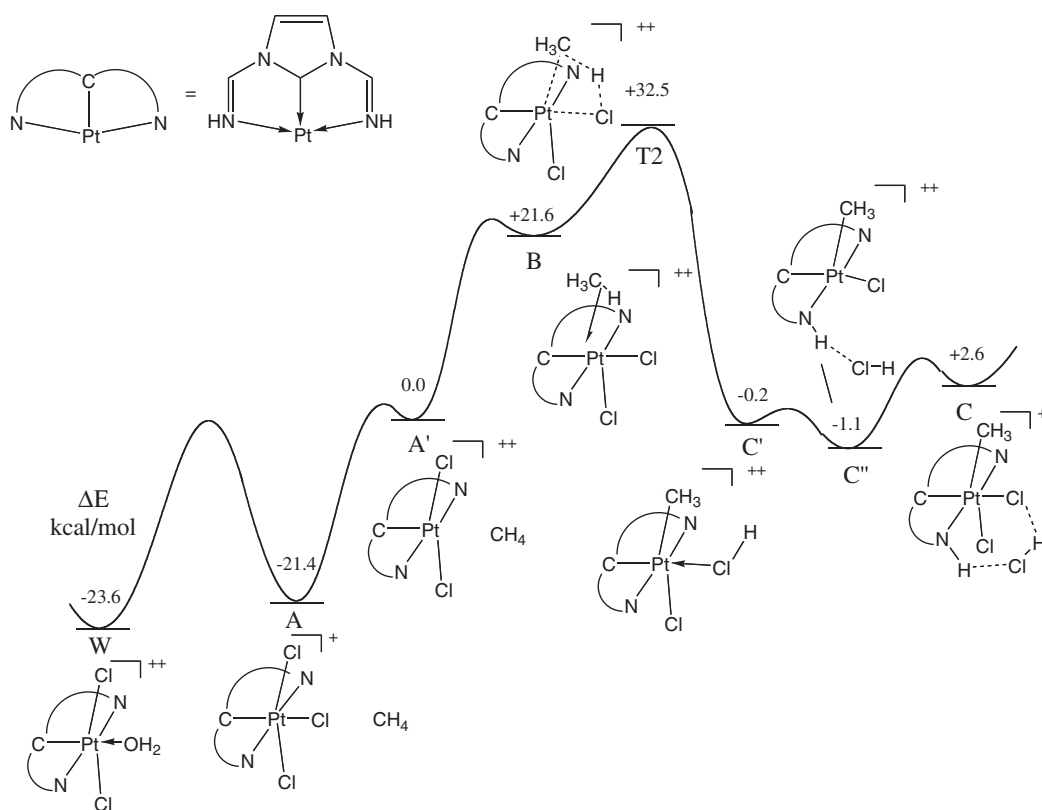


Figure 15. A similar ligand system to the previous figure. This one has a favorable activation barrier, but is not resistant to water poisoning.

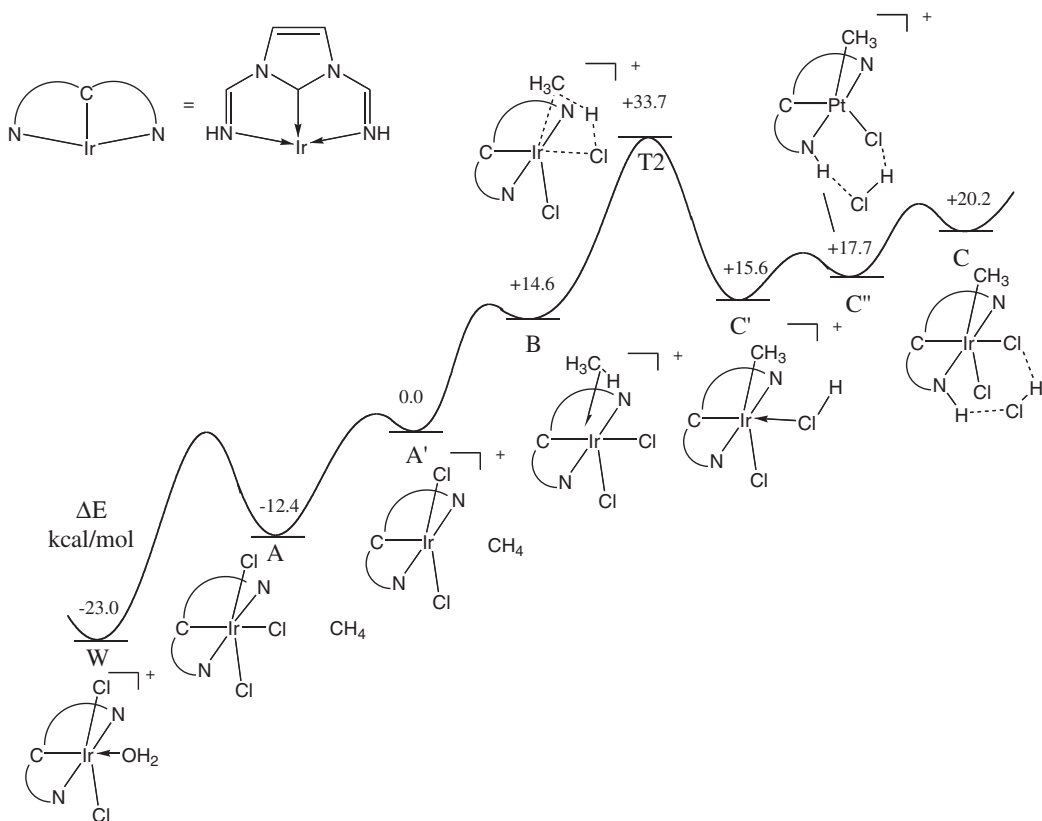


Figure 16. A NCN Ir (III) system that passes QM-RP tests 1 and 2, but is not resistant to water.

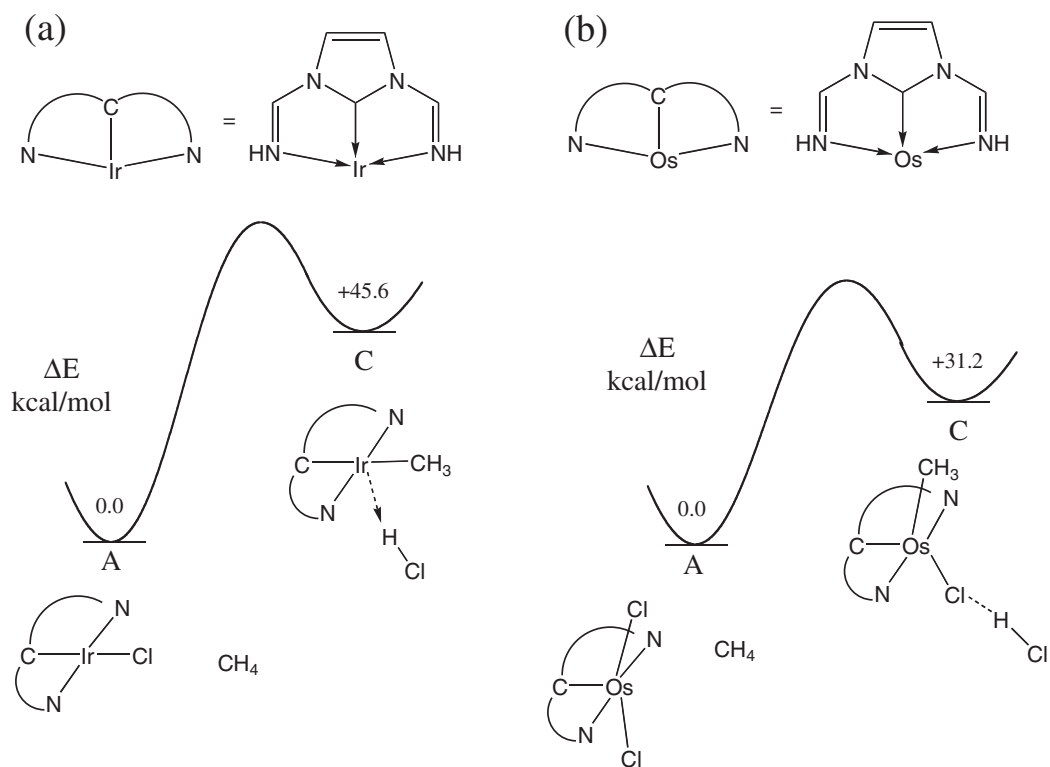
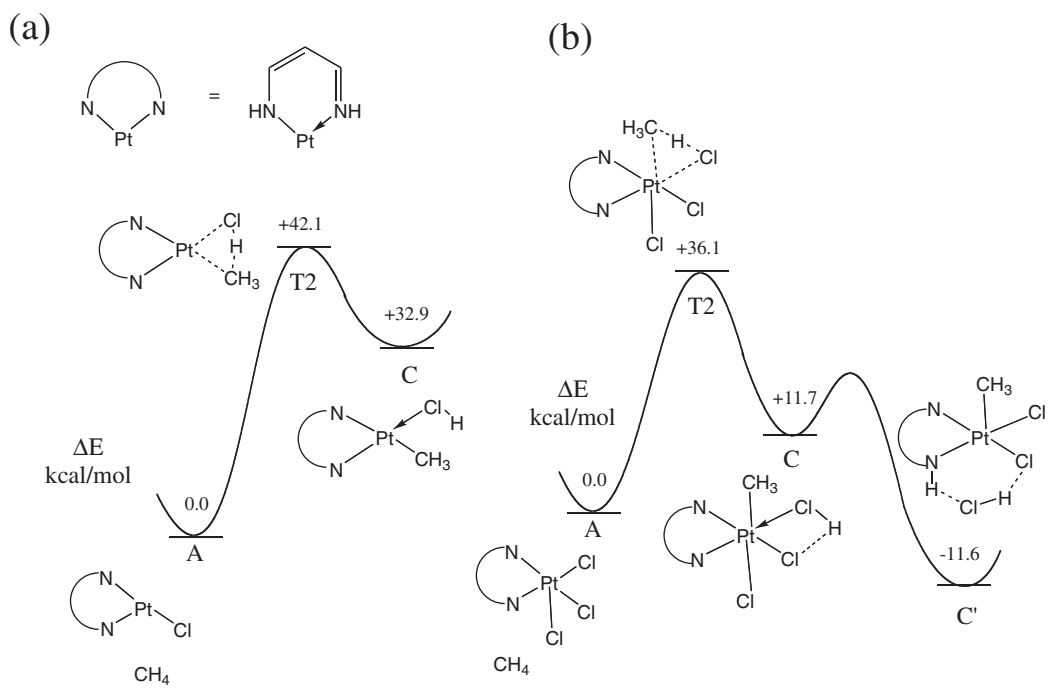


Figure 17. NCN Ir(I) and Os(II) systems. These do not pass QM-RP test 1.



Note: Other permutations for A, C, and T2 connecting them led to higher energy pathways.

Figure 18. Resonating bidentate ligands for Pt(II) and Pt(IV). The Pt(IV) system has favorable energetics.

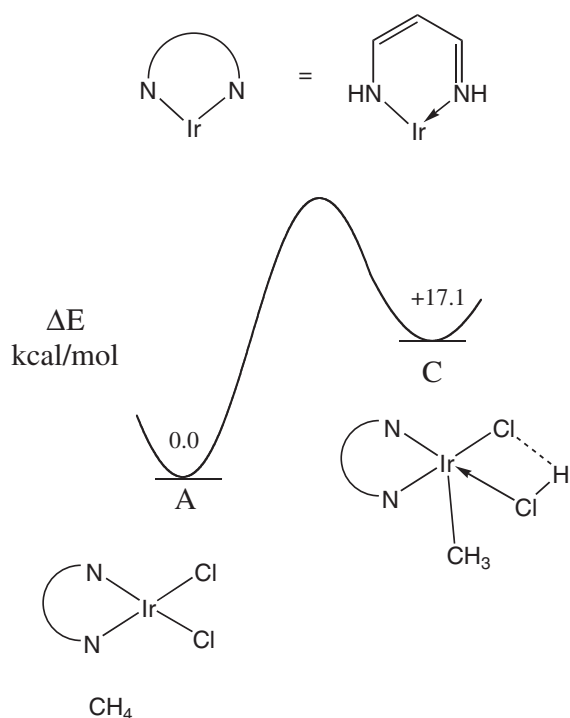


Figure 19. Resonating bidentate ligands for Ir (III); this system does not pass QM-RP test 1.

6. Conclusion

This paper describes the QM-RP technique we have developed at Caltech in the Materials and Process Simulation Center to develop new catalysts. This has been applied successfully to the development of polymerization catalysts for polar olefins and to catalysts for methane activation. For the latter case, we focus on the C–H bond activation step, first looking for a system with favorable energetics to bond to methyl radical (QM-RP test 1), then looking for systems that are resistant to poisoning by water (QM-RP test 2), and then looking for systems with favorable barriers to forming the M–CH₃ bond (QM-RP test 3). These are the most severe tests. Then, we examine whether oxidation and functionalization steps are favorable (QM-RP test 4). This work has identified interesting new candidates that are being studied experimentally.

We have emphasized in this example the quantitative results; however, the interpretation of the results to develop a qualitative understanding of why particular results are obtained is equally important. It is this qualitative understanding that suggests bold new systems rather than small perturbative iterations. Thus, in the QM studies, we focus on extraction of an understanding of how the electronic influences at the

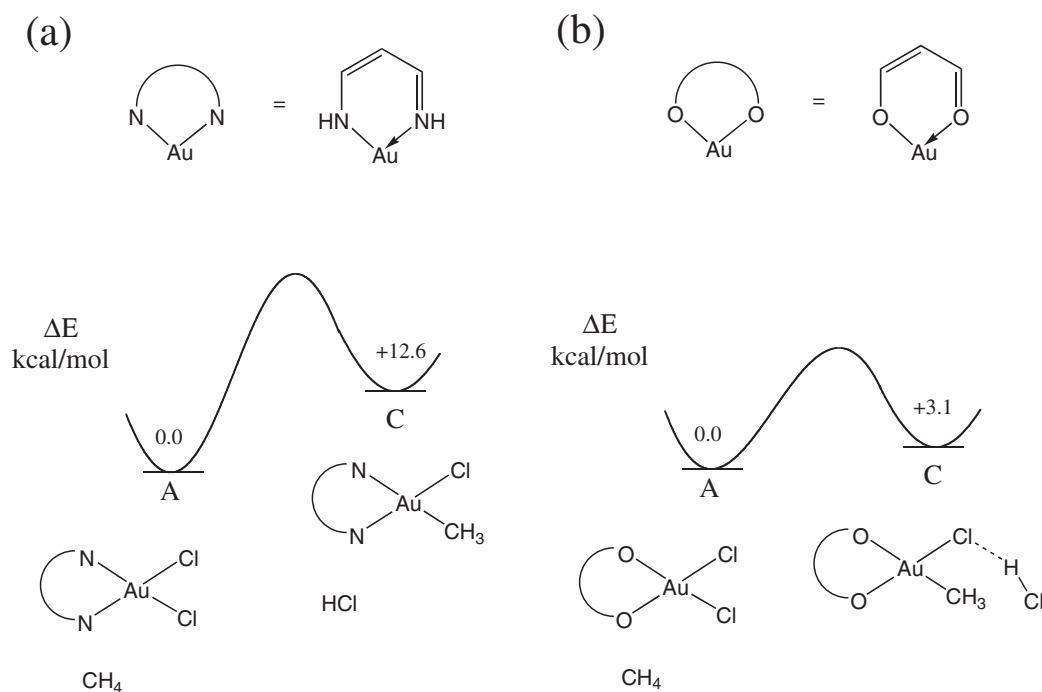
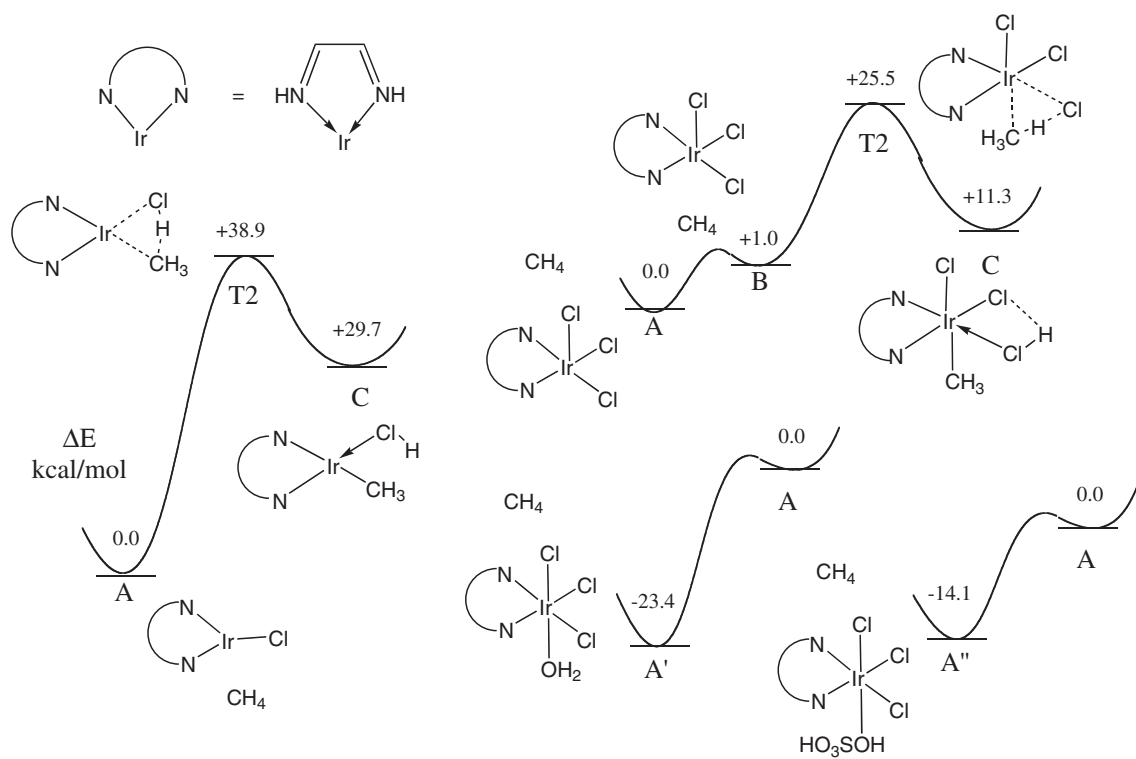


Figure 20. Resonating bidentate ligands for Au (III) with very favorable energetics.



Note: Other permutations for A, C, and T2 connecting them led to higher energy pathways.

Figure 21. Ir (I), (III), and (V) systems with classic Brookhart bidentate ligands.

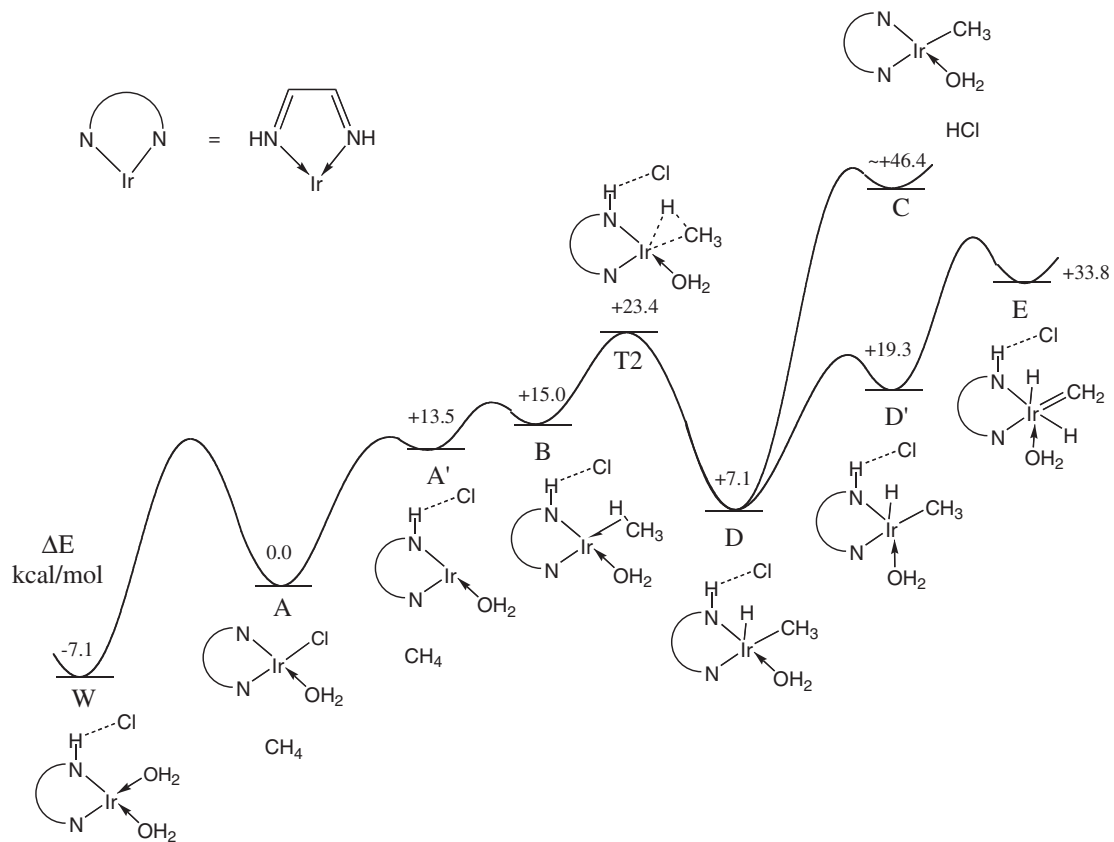


Figure 22. Poisoning by water of Ir (I) system with a bidentate ligand.

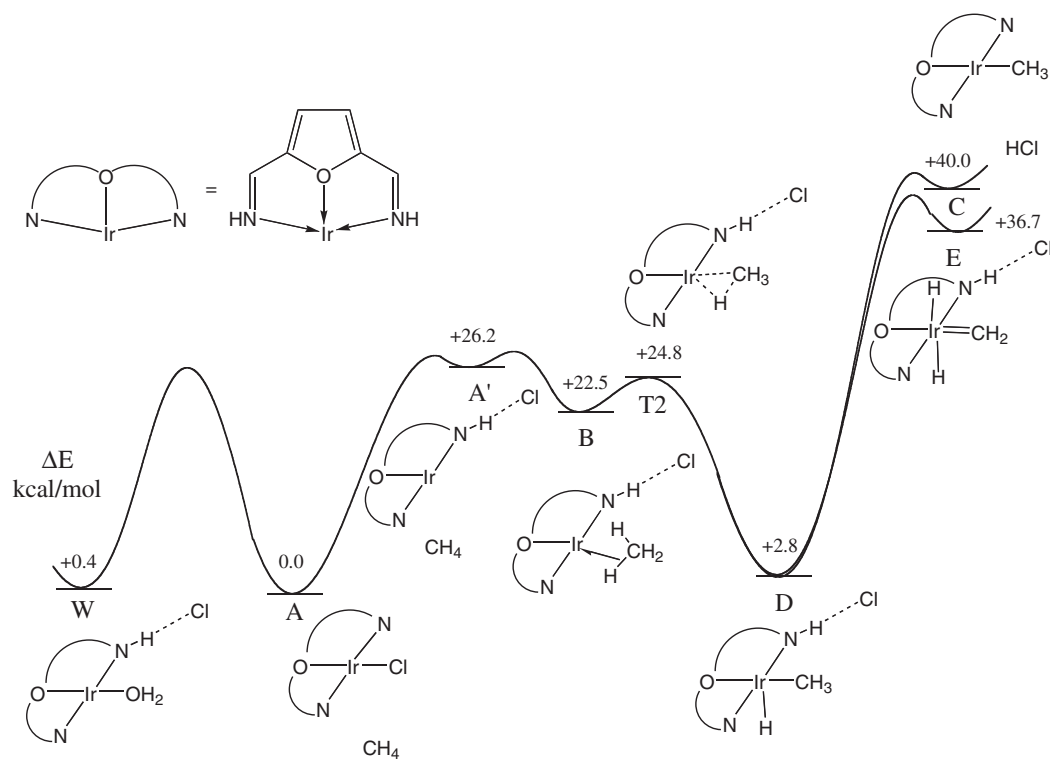


Figure 23. Ir (I) system that is resistant to water poisoning and which forms a compound to methylene.

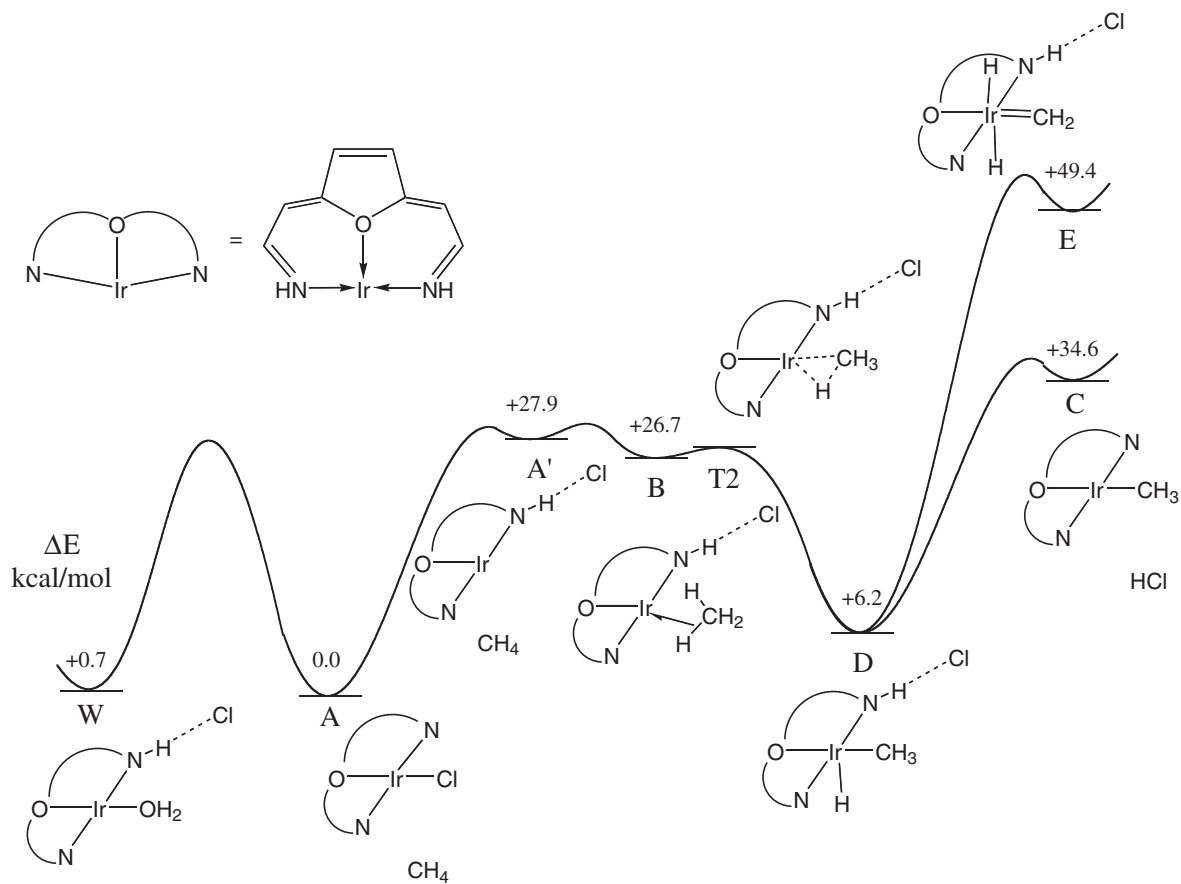


Figure 24. Ir (I) system that is resistant to water and forms a bond to methyl with very favorable energetics overall.

transition metal center affect the energetics of the relevant catalytic steps.

Acknowledgments

We thank Prof. Roy Periana of USC and Dr. Bill Schinski of ChevronTexaco for many helpful discussions. This work was partially supported by Chevron-Texaco and by NSF-CHE. The facilities of the MSC were funded by NSF-CHE, ARO/DURIP, ONR/DURIP, and a SUR grant from IBM. In addition, the MSC is supported by grants from DOE-ASCI, ARO/MURI, ONR/MURI, the NIH, ONR, General Motors, Seiko-Epson, Beckman Institute, and Asahi Kasei.

References

- [1] F.S. Bates and G.H. Fredrickson, *Annu. Rev. Phys. Chem.* 41 (1990) 525.
- [2] B.A. Arnsteden, R.G. Bergman, T.A. Mobley and T.H. Peterson, *Acc. Chem. Res.* 28 (1995) 154.
- [3] S.E. Bromberg, H. Yang, C.M. Asplund, T. Lian, K.B. McNamara, K.T. Kotz, J.S. Yeston, M. Wilkens, H. Frei, R.G. Bergman and C.B. Harris, *Science* 278 (1997) 260.
- [4] J.A. Davies, P.L. Watson, J.L. Liebman and A. Greenberg (eds.), *Selective Hydrocarbon Activation* (Wiley-VCH, New York, 1990).
- [5] C. Hall and R.N. Perutz, *Chem. Rev.* 96 (1996) 3125.
- [6] C.L. Hill, *Activation and Functionalization of Alkanes* (Wiley-Interscience, New York, 1989).
- [7] A. Sen, *Acc. Chem. Res.* 21 (1988) 421.
- [8] A.E. Shilov and G.B. Shul'pin, *Chem. Rev.* 97 (1997) 2879.
- [9] J. Sommer and J. Bukala, *Acc. Chem. Res.* 26 (1993) 370.
- [10] K.M. Walktz and J.F. Hartwig, *Science* 277 (1997) 211.
- [11] M. Muthukumar, C.K. Ober and E.L. Thomas, *Science* 277 (1997) 1225.
- [12] C.K. Ober and G. Wegner, *Adv. Mater.* 9 (1997) 17.
- [13] R.A. Periana, D.J. Taube, E.R. Evitt, D.G. Löffler, P.R. Wentreck, G. Voss and T. Masuda, *Science* 259 (1993) 340.
- [14] R.A. Periana, D.J. Taube, S. Gamble, H. Taube, T. Satoh and H. Fujii, *Science* 280 (1998) 560.
- [15] M. Ringnalda *et al.*, Jaguar v4.0 (Schrödinger, Inc., Portland, OR, 2000).
- [16] J.C. Slater, *Quantum Theory of Molecules and Solids, Vol. 4: The Self-Consistent Field for Molecules and Solids* (McGraw-Hill, New York, 1974).
- [17] A.D. Becke, *J. Chem. Phys.* 98 (1993) 5648.
- [18] A.D. Becke, *Phys. Rev. A* 38 (1988) 3098.
- [19] S.H. Vosko, L. Wilk and M. Nusair, *Can. J. Phys.* 58 (1980) 1200.
- [20] C.T. Lee, W.T. Yang and R.G. Parr, *Phys. Rev. B* 37 (1988) 785.
- [21] P.J. Hay and W.R. Wadt, *J. Chem. Phys.* 82 (1985) 299.
- [22] D.J. Tannor, B. Marten, R. Murphy, R.A. Friesner, D. Sitkoff, A. Nicholls, M. Ringnalda, W.A. Goddard and B. Honig, *J. Am. Chem. Soc.* 116 (1994) 11875.
- [23] B. Marten, K. Kim, C. Cortis, R.A. Friesner, R.B. Murphy, M.N. Ringnalda, D. Sitkoff and B. Honig, *J. Phys. Chem.* 100 (1996) 11775.
- [24] C.M. Cortis and R.A. Friesner, *J. Comput. Chem.* 18 (1997) 1570.
- [25] D.M. Philipp, R.P. Muller, W.A. Goddard III, J. Storer, M. McAdon and M. Mullins, *J. Am. Chem. Soc.* 124 (2002) 10198.
- [26] J.K. Klassen, K.M. Fieher and G.M. Nathanson, *J. Phys. Chem. B* 101 (1997) 9098.
- [27] X. Xu, J. Kua, R.A. Periana, and W.A. Goddard, *Organometallics* 22 (2003) 2057.
- [28] D.R. Lide, *CRC Handbook of Chemistry and Physics*, 74th edition (CRC Press, Boca Raton, FL, 1993–94).